

LARGE-SCALE [C II] 158 MICRON EMISSION FROM THE GALAXY

HIROSHI SHIBAI, HARUYUKI OKUDA, AND TAKAO NAKAGAWA

The Institute of Space and Astronautical Science, 3-1-1, Yoshino-dai, Sagami-hara, Kanagawa 229, Japan

HIDEO MATSUHARA

Department of Astrophysics, Nagoya University, Furo-cho, Chikusa-ku, Nagoya 464, Japan

TOSHINORI MAIHARA AND KOHEI MIZUTANI

Department of Physics, Kyoto University, Kitashirakawa, Sakyo-ku, Kyoto 606, Japan

YUKIYASU KOBAYASHI

Institute of Astronomy, University of Tokyo, 2-21-1, Osawa, Mitaka, Tokyo 181, Japan

NORIHISA HIROMOTO

Communications Research Laboratory, 4-2-1, Nukui-Kitamachi, Koganei, Tokyo 184, Japan

AND

TETSUO NISHIMURA AND FRANK J. LOW

Steward Observatory, University of Arizona, Tucson, AZ 85721

Received 1990 January 30; accepted 1990 December 11

ABSTRACT

A diffuse far-infrared [C II] emission line has been detected in an extensive region ($30^\circ \leq l \leq 51^\circ$) along the Galactic plane. The [C II] line is bright and extended far from discrete luminous H II regions. Latitudinal and longitudinal profiles of the [C II] intensity distribution are quite similar to those of $^{12}\text{CO}(J=1-0)$ and the $100\ \mu\text{m}$ continuum, but are completely different from those of H I 21 cm. The diffuse [C II] emission probably comes from the photodissociated C^+ regions enveloping giant molecular clouds exposed to the general interstellar UV radiation field. The extended low-density ionized gas might also contribute to the diffuse [C II] emission. The mass of the C^+ regions may be as much as 35%–50% of that of CO molecular gas. The total luminosity of the [C II] line emitted from the inner Galactic disk amounts to $2.8(\pm 1.1) \times 10^7 L_\odot$, or about $0.36_{-0.17}^{+0.28}\%$ of the total far-infrared luminosity of the same region.

Subject headings: atomic processes — galaxies: structure — galaxies: The Galaxy — infrared: spectra — interstellar: abundances — interstellar: matter

1. INTRODUCTION

The fine-structure line of [C II] $^2P_{3/2}-^2P_{1/2}$ at $157.741\ \mu\text{m}$ (Cooksy, Blake, & Saykally 1986) has recently been detected in a number of Galactic and extragalactic objects and has played important roles in studying warm interfaces between molecular clouds and H II regions. These interface regions are often termed “photodissociation regions” (de Jong, Dalgarno, & Boland 1980; Tielens & Hollenbach 1985; Genzel, Harris, & Stutzki 1989). A large part of the observational efforts to date have been concentrated on studies of the dense photodissociation regions found at the interfaces between dense molecular clouds and Galactic H II regions.

Recently, a few authors (Russell et al. 1981; Kurtz et al. 1983; Stutzki et al. 1988; Matsuhara et al. 1989, 1990) detected diffuse [C II] emission extended around the Galactic H II regions. The extended [C II] emission is weaker in terms of intensity but much more widely distributed than the [C II] emission from the H II region interface. On the other hand, Stacey et al. (1985) detected strong [C II] emission in the Galactic plane at $l = 2^\circ 16', 7^\circ 29'$ and $7^\circ 80'$, regions specifically chosen to be devoid of discrete H II regions. They found their [C II] latitudinal profiles to be similar to those of $^{12}\text{CO}(J=1-0)$. Crawford et al. (1985) showed a similarly good correlation between [C II] and $^{12}\text{CO}(J=1-0)$ intensities and distributions for several external galaxies. These authors concluded that the observed [C II] emission arises from photodissociation regions formed on the surfaces of giant molecular clouds exposed to

the ultraviolet radiation fields of embedded OB stars or the general interstellar ultraviolet radiation fields. The observations of Stacey et al. (1985), however, have too limited sky coverage to permit detailed studies of the [C II] line emission from the Galaxy. We therefore decided to pursue large-scale mapping of the [C II] line.

We describe the Galactic [C II] distribution observed with our balloon-borne system in § 3, [C II] intensities expected for the representative interstellar gases in § 4, and discussions for the diffuse [C II] emission in § 5. We assumed throughout this paper that the distance to the Galactic center is 8.5 kpc; referred distances and luminosities that had been derived on the assumption of 10 kpc to the Galactic center have been multiplied by 0.85 and $(0.85)^2$, respectively.

2. INSTRUMENTS AND OBSERVATIONS

The observations reported here were made using the Balloon-Borne Infrared Telescope (BIRT), which is a 50 cm diameter telescope with an altitude-azimuthal pointing system (Okuda et al. 1984; Shibai et al. 1990) and a liquid-helium-cooled Fabry-Perot spectrometer (Okuda et al. 1986; Nakagawa et al. 1990) with a stressed Ge:Ga detector (Hiromoto et al. 1989). A circular beam of $3/4$ (FWHM) or $3/7$ (equivalent disk) diameter was used. The system noise-equivalent power including all optical losses during the observations was about $10^{-14}\ \text{W Hz}^{-1/2}$. The spectral resolving power was 2100 ($143\ \text{km s}^{-1}$).

In order to detect extended [C II] line emission accurately and efficiently, the frequency (wavelength) switching technique (Matsuhara et al. 1989; Nakagawa et al. 1990), instead of the conventional spatial chopping, was used for the background cancellation. The velocity resolution (143 km s^{-1}) and the switching spans ($\pm 175 \text{ km s}^{-1}$) were not large compared with the velocity dispersion of the Galactic plane ($\sim \pm 200 \text{ km s}^{-1}$). Thus the efficiency of line detection depends on the spectral profiles and positions of the line. Using the intrinsic spectral response profile of the spectrometer and the wavelength differences between the expected line position (estimated through CO profiles in Sanders et al. 1986) and the center positions of the frequency switching, we estimated the relative efficiencies, η_V , for the objects, shown in Table 1 together with their estimated errors. We have confirmed that the estimated efficiencies are consistent with observational values for M17 (Matsuhara et al. 1989) and NGC 6334 (Nakagawa et al. 1991) by observing with both the conventional spectral scanning mode and the frequency switching mode. Through observations of Mars we confirm that far-infrared continuum emission does not contaminate the observed line intensities.

Two balloon flights were made from the National Scientific Balloon Facility (NSBF), Palestine, Texas, on 1988 May 24–25 and June 4–5. The observational data of the present work were acquired from several short-period measurements in the two flights. The total observation time was about 3 hr. In-flight calibration of the sensitivity was achieved by the same method described by Matsuhara et al. (1989). The uncertainty of the absolute intensity is estimated to be less than $\pm 30\%$.

The observations consisted of two parts: nighttime and daytime observations. In the nighttime observations the telescope direction was determined relative to known visible stars by an on-board star sensor, so the positional uncertainties are small, less than $1'$. Regions near W43 ($l = 30^\circ 8'$) and NGC 6334 ($l = 351^\circ 4'$) were observed. The scan paths are displayed on the 6 cm radio continuum maps (Haynes, Caswell, & Simmons 1978) in Figures 1b and 2b. The center spectral position was set at $+65 \text{ km s}^{-1}$ (LSR) for W43 and at -70 km s^{-1} (LSR) for NGC 6334 (Table 1). The relative efficiency of the frequency switching, η_V , is estimated to be $84(\pm 9\%)$ for W43 and around 40% for NGC 6334.

The star sensor is not usable for daytime observations, so the positional accuracy of these observations is determined by the accuracy of a geomagnetic sensor, $\sim 5'$. The center spectral position was set at $+65 \text{ km s}^{-1}$ for $l < 42^\circ$ and at $+20 \text{ km s}^{-1}$ for $l > 42^\circ$ to detect the major Galactic components as fully as possible. The relative efficiencies, η_V , in the daytime observations are also shown in Table 1. Thirty-one azimuthal raster

scans and two elevational scans were obtained, which cover the Galactic plane (undersampled) from $l = 30^\circ$ to $l = 51^\circ$. The paths of our cuts are illustrated by the light lines in Figure 3.

3. RESULTS

3.1. W43 and NGC 6334

Figures 1a and 2a show the [C II] intensity profiles along the scan paths crossing the Galactic plane at W43 ($l = 30^\circ 8'$) and near NGC 6334 ($l = 351^\circ 4'$). The data have been averaged in $2'$ bins for W43 and $4'$ bins for NGC 6334, and error bars indicate 1 standard deviation from the mean. The zero flux level has been determined from the average level of the data in $1^\circ 2' < |b| < 1^\circ 5'$ and in $1^\circ 5' < |b| < 3^\circ$ for W43 and NGC 6334, respectively, assuming the line flux here is zero.

The peak intensity of the W43 scan is $9 \times 10^{-4} \text{ ergs cm}^{-2} \text{ s}^{-1} \text{ sr}^{-1}$ (not corrected for η_V), and the FWHM is about 1° . The peak position coincides (to within the beam size) with the positions of radio continuum and far-infrared peaks. It is not clear from this profile only whether or not the [C II] profile can be resolved into narrow features and an extended component or not. However, as the spatial extent of the narrow feature at the peak of the [C II] intensity ($\sim 10'$) is similar to the far-infrared continuum extent (Lester et al. 1985), we associate this

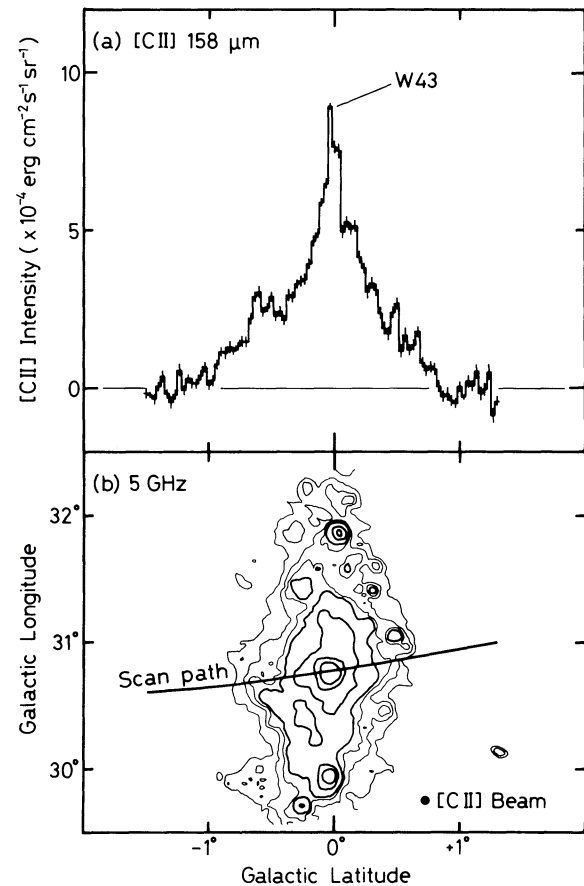


FIG. 1.—(a) [C II] line intensity profile crossing W43. The center frequency of the switching was set at $V(\text{LSR}) = +65 \text{ km s}^{-1}$. The integrating bin is $2'$, and the error bars represent $\pm 1 \sigma$ errors. The beam size ($3/4'$) and the scan path are displayed in (b) together with a 5 GHz radio continuum map (Haynes et al. 1978). Contour levels of 5 GHz correspond to 0.4, 0.6, 0.8, 1, 2, 4, 8, 12, 16, and 20 K. The [C II] scan has not been corrected for the relative switching efficiency, η_V .

TABLE 1

ESTIMATED RELATIVE EFFICIENCIES OF FREQUENCY SWITCHING

Object	$V(\text{LSR})^a$ (km s^{-1})	$V(\text{FSW})^b$ (km s^{-1})	η_V (%)
W43	$+92.3^\circ$	$+65 \pm 10$	84 ± 9
NGC 6334	-2.5°	-70 ± 10	40 ± 11
Galactic plane ^d			
$30^\circ < l < 42^\circ$	$+40$ to $+110$	$+65 \pm 10$	75 ± 20
$42^\circ < l < 51^\circ$	$+20$ to $+70$	$+20 \pm 10$	70 ± 20

^a LSR velocity of the object.

^b LSR velocity corresponding to the center position of the switching.

^c Referred to Reifenstein et al. 1970.

^d Major Galactic components.

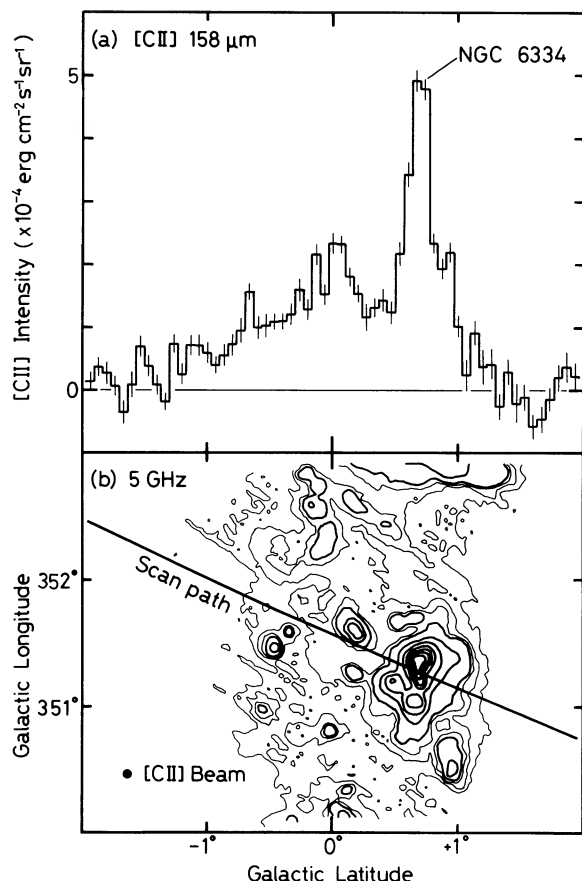


FIG. 2.—(a) [C II] line intensity profile crossing NGC 6334. The center frequency of the switching was set at $V(\text{LSR}) = -70 \text{ km s}^{-1}$ in $V(\text{LSR})$. The integrating bin is $4'$. (b) 5 GHz radio continuum map (Haynes et al. 1978) and the scan path of the [C II] observation. Other parameters are the same as in Fig. 1.

feature with W43. The broad feature (FWHM $\sim 1^\circ$) in the [C II] distribution may be ascribed to an extended “halo” of W43 or to background [C II] emission from the Galactic plane.

Similarly, the peak of the [C II] line emission in the NGC 6334 scan (Figure 2a) coincides with the 5 GHz radio continuum peak. Other features in the 5 GHz map, particularly the H II region G351.6+0.2 (Haynes, Caswell, & Simons 1979; McBreen, Jaffe, & Fazio 1983) are also reproduced in the [C II] scan. However, there remains relatively strong [C II] emission over a much larger region than may be ascribed to these two radio continuum peaks. Therefore, as for W43 above,

there remains an extended “halo” of [C II] line emission from NGC 6334 which is more widely distributed than the local H II regions.

3.2. [C II] Emission from $30^\circ \leq l \leq 51^\circ$

Figure 3 displays a two-dimensional distribution of the [C II] intensity along the Galactic plane, obtained by the daytime observations. The [C II] profile along each scan path was smoothed by the running mean of $10'$ span to increase signal-to-noise ratio (S/N), and, after that, equal intensity points of the adjacent scan paths were successively traced. Each contour step corresponds to $10^{-4} \text{ ergs cm}^{-2} \text{ s}^{-1} \text{ sr}^{-1}$. The data have not been corrected for the relative switching efficiency, η_V (listed in Table 1). The ambiguity of the zero flux level is $\pm 0.5 \times 10^{-4} \text{ ergs cm}^{-2} \text{ s}^{-1} \text{ sr}^{-1}$, which corresponds to half the contour interval.

The diffuse [C II] emission is widely distributed along the Galactic plane from $l = 30^\circ$ to $l = 51^\circ$. Typical full widths in latitude are 1° – 2° . The extended [C II] emission components seen in Figures 1a and 2a may be understood as a part of this large-scale [C II] emission component in the inner Galactic disk.

There is extended [C II] line emission from the regions around W43, of size $\Delta l \sim 2^\circ$ (from 30° to 32°) and $\Delta b \sim 1^\circ$ (from -0.5 to $+0.5$). We will refer to this as the “31° region.” Some other [C II] peaks are evidently associated with the active star-forming regions, e.g., W49 ($l = 43^\circ$) and W51 ($l = 49^\circ$).

3.3. Comparison of Latitudinal Profile with Other Tracers

The latitudinal profile of the [C II] intensity along the scan path across W43 is compared with the tracers of molecular gas [$^{12}\text{CO}(J = 1-0)$], dust (far-infrared [$100 \mu\text{m}$] continuum), ionized gas (5 GHz radio continuum), and atomic gas (H I 21 cm) in Figure 4. The [C II] intensity has been corrected for the relative switching efficiencies, $\eta_V = 0.84$ (Table 1). The [$^{12}\text{CO}(J = 1-0)$] profile (Fig. 4a) was obtained by integration of the Massachusetts–Stony Brook Galactic Plane CO Survey (Sanders et al. 1986) over the LSR velocity between -50 and $+150 \text{ km s}^{-1}$. This velocity coverage includes almost all of the major components of the inner Galactic disk at $l = 30^\circ$. The $100 \mu\text{m}$ far-infrared continuum profile (Fig. 4b) was constructed from the $100 \mu\text{m}$ map of *IRAS Galactic Plane Images* (1985, as described in the *IRAS Explanatory Supplement* 1985). The 5 GHz radio continuum profile (Fig. 4c) was reconstructed from the Parkes 5 GHz map of Haynes et al. (1978). The H I 21 cm integrated intensity profile (Fig. 4d) was obtained by integrating the Leiden–Green Bank survey data (Burton 1985) from -200 to $+200 \text{ km s}^{-1}$. The data for CO, the far-infrared

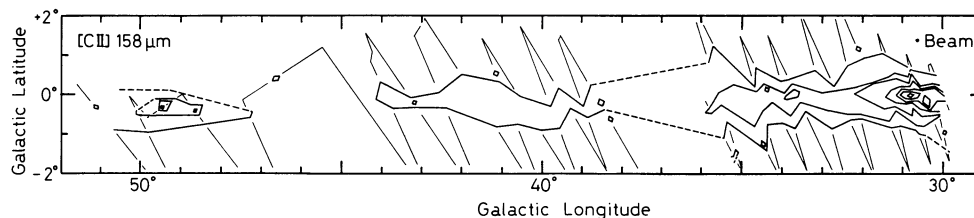


FIG. 3.—Large-scale [C II] line intensity distribution along the Galactic plane. The scan paths are displayed with thin solid lines, and the beam size ($3/4'$) is displayed at the upper right-hand corner. The data are smoothed to lie along the scan path so that the effective beam size is $10'$. Spans among the adjacent scan paths are more than several times the width of the beam. The contour intervals are $10^{-4} \text{ ergs cm}^{-2} \text{ s}^{-1} \text{ sr}^{-1}$. The center frequency of switching was set at $+65 \text{ km s}^{-1}$ for $l < 42^\circ$ and at $+20 \text{ km s}^{-1}$ for $l > 42^\circ$. The data have not been corrected for the relative switching efficiency, η_V .

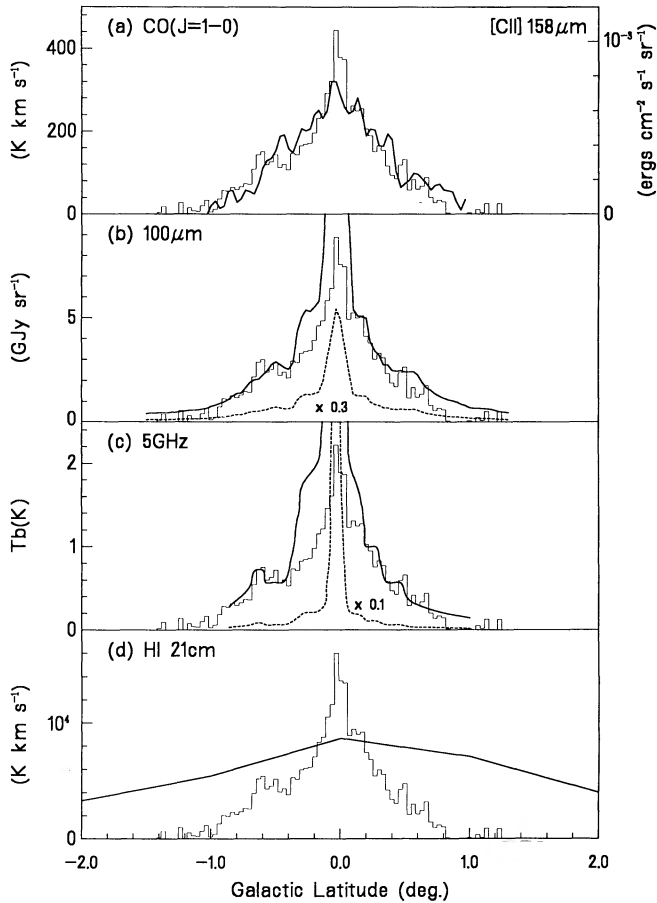


FIG. 4.—(a) [C II] profile across W43 superposed on the latitudinal profile of the $^{12}\text{CO}(J=1-0)$ integrated line intensity. The CO data were integrated over velocities between -50 and 150 km s^{-1} (Sanders et al. 1986), and the [C II] data have been scaled up by the relative switching efficiency, $\eta_r = 0.84$. (b) [C II] scan superposed on the *IRAS* $100 \mu\text{m}$ band (*IRAS* Galactic Plane Images). (c) [C II] scan superposed on the 5 GHz radio continuum (Altenhoff et al. 1978). (d) [C II] scan superposed on the H I 21 cm (Burton 1985) integrated line intensity. Except for H I 21 cm, all of the profiles were produced from data along the same scan path as that of [C II] shown in Fig. 2a. That of H I was made from the integrated intensities along $l = 31^\circ$. The ordinate scales of the [C II] are the same for these four panels.

(FIR) and 5 GHz were taken along the same scan path as those of the [C II] data (Fig. 1b), but the H I data are a cut across Galactic longitude $l = 31^\circ$.

The ordinate scales of [C II] are the same in the panels of Figure 4. Those of CO, FIR, and 5 GHz were determined so as to get the best fit in $|b| > 0.3$. Since the same way of fitting for H I is impossible because of poor correlation between [C II] and H I, the scale was determined so as to obtain agreement around $b = 0^\circ$, seen in Figure 4d. In this manner, the ratios of

the [C II] intensity to other tracers were obtained and are listed in Table 2, where the upper and lower bounds were originated from calibration uncertainties of each tracer; $\pm 30\%$ for [C II], $\pm 20\%$ for $100 \mu\text{m}$, and $\pm 10\%$ for CO, 5 GHz, and H I (given in each reference).

The latitudinal profile of [C II] is quite similar to that of ^{12}CO (Fig. 4a). Only small differences are seen; the [C II] profile has a distinct narrow peak at W43 relative to the CO profile, and the relative intensity ratio seems to be somewhat different on either side of the Galactic equator. The intensity ratio of the [C II] line to the CO line in Table 2 corresponds to a line luminosity ratio of 1500_{-600}^{+700} . The similar spatial distribution of [C II] and CO was found by Stacey et al. (1985) for their Galactic longitude cuts at $l = 2^\circ 16'$, $7^\circ 29'$, and $7^\circ 80'$ and by Crawford et al. (1985) for several external galaxies.

The 60 and $100 \mu\text{m}$ *IRAS* far-infrared continuum has a similar latitudinal profile to that of [C II] (Fig. 4b) except near the W43 peak, which is strongly enhanced in the far-infrared. The mean flux ratio of $100 \mu\text{m}/60 \mu\text{m}$ along the scan path is about 4, except near the W43 peak. The total far-infrared luminosity can be obtained from *IRAS* 60 and $100 \mu\text{m}$ fluxes assuming a single-temperature thermal emission model with grain emissivity $\sim \lambda^{-n}$ (*IRAS* Cataloged Galaxies and Quasars 1985, Appendix B). Assuming $n = 1$ or 2 and using the observed intensity ratio (Table 2), the intensity ratio of the [C II] $158 \mu\text{m}$ to the total far-infrared emission is $0.58_{-0.24}^{+0.34}\%$.

The radio continuum is similarly well correlated with the [C II] at $|b| > 0.3$ but also is clearly enhanced at the location of the H II region, W43.

In contrast to these similarities, the latitudinal profile of H I 21 cm is considerably wider than that of [C II] as well as other tracers (Fig. 4d). The H I is clearly not correlated with the other tracers in this latitudinal profile.

We conclude, from these facts, that the diffuse [C II] correlates well over the Galactic plane with the tracers of the molecular and ionized gas and dust, but not with the tracers of the atomic medium. This correlation apparently breaks down near H II regions.

3.4. Longitudinal Distribution

The [C II] intensity data shown in Figure 3 have been integrated along each scan path to derive the longitudinal profile of [C II], and the result is shown in Figure 5a. Error bars indicate the uncertainties due primarily to the ambiguity of the zero-level determination and of the absolute calibration. The integrated intensity of the scan across NGC 6334 is not included in this figure, since its larger correction for the relative switching efficiency may introduce large errors (Table 1). The data taken from Stacey et al. (1985) were also plotted after integrations in the same manner. The solid line shows the result of three linear fits to the [C II] longitudinal profile. The regions fitted are $l \leq 30^\circ$; $30^\circ \leq l \leq 39^\circ$; $39^\circ \leq l$.

TABLE 2
INTENSITY RATIOS OF [C II] TO OTHER TRACERS^a

Ratio	Value
[C II]/ $^{12}\text{CO}(J=1-0)$	$2.4_{-0.9}^{+1.1} \times 10^{-6}$ (ergs $\text{cm}^{-2} \text{s}^{-1} \text{sr}^{-1}$)/(K km s^{-1})
[C II]/FIR ($100 \mu\text{m}$)	$1.2_{-0.3}^{+0.7} \times 10^{-13}$ (ergs $\text{cm}^{-2} \text{s}^{-1} \text{sr}^{-1}$)/(Jy sr^{-1})
[C II]/Radio (5 GHz)	$4.8_{-1.7}^{+2.1} \times 10^{-4}$ (ergs $\text{cm}^{-2} \text{s}^{-1} \text{sr}^{-1}$)/K
[C II]/H I (21 cm)	$6.7_{-2.4}^{+3.0} \times 10^{-7}$ (ergs $\text{cm}^{-2} \text{s}^{-1} \text{sr}^{-1}$)/(K km s^{-1})

^a See text.

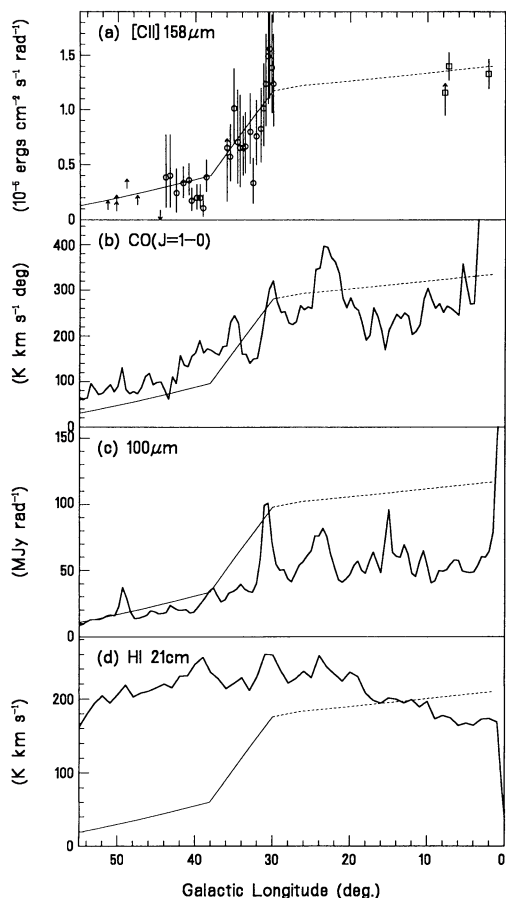


FIG. 5.—(a) Longitudinal distribution of the integrated [C II] line intensity. The open circles with error bars in $l > 30^\circ$ indicate the data points of this work. Error bars are determined mainly by uncertainties of the zero intensity level. The open squares with error bars indicate the data of Stacey et al. (1985). The solid and dashed lines represent a best-fit linear longitudinal profile, where the dashed line indicates interpolation between the data of this work and those of Stacey et al. (1985). [C II] distribution compared with (b) $^{12}\text{CO}(J = 1-0)$ distribution (Dame et al. 1987), (c) *IRAS* 100 μm distribution (*IRAS* Low-Resolution Maps), and (d) H I 21 cm distribution (Burton 1985). The H I intensity is proportional to the column densities of atomic hydrogen along the Galactic equator, and the profiles of $^{12}\text{CO}(J = 1-0)$ and *IRAS* 100 μm are the intensities integrated over the Galactic latitude within $|b| < 1^\circ$ and $|b| < 5^\circ$, respectively.

The [C II] integrated intensity at $l = 30^\circ$ agrees with that of $l = 2^\circ 16'$, $7^\circ 29'$, and $7^\circ 80'$ obtained by Stacey et al. (1985). Beyond $l = 30^\circ$, however, the [C II] intensity decreases rapidly. The direction of $l = 30^\circ$ is the tangential point of the 4 kpc molecular ring. If these data represent the large-scale [C II] emission of the Galaxy, then this rapid falloff implies that the [C II] emission is more intense at or within the 4 kpc ring than the inner or outer regions of the Galaxy.

3.5. Comparison of Longitudinal Profiles with Other Tracers

In Figures 5b, 5c, and 5d, longitudinal profiles of $^{12}\text{CO}(J = 1-0)$, far-infrared (100 μm) continuum, and H I 21 cm are compared with that of [C II]. The ordinate scales of these three figures are scaled by the flux ratios determined over $|b| > 0.3^\circ$ in § 3.3.

The longitudinal profile of CO (Fig. 5b) is taken from the Columbia survey (Dame et al. 1987). The intensities have been integrated over all velocities and over Galactic latitude within

$|b| < 10^\circ$. The far-infrared continuum profile (Fig. 5c) was obtained by integrating the data of *IRAS Low-Resolution Maps* (1985, as described in the *IRAS Explanatory Supplement* 1985) over latitudes less than 1° . The H I 21 cm profile was obtained from the Leiden-Green Bank survey (Burton 1985) after integrating in LSR velocity within $\pm 200 \text{ km s}^{-1}$. The thin lines in these figures are the same as that of Figure 5a, the fitted [C II] profile.

As for the latitudinal profile, the longitudinal profile of the [C II] resembles those of CO and the FIR. The [C II] profile has a particularly good correlation, even on a small scale, with that of CO. For instance, the peaks at $l = 31^\circ$ and 35° and the dip at $l = 33^\circ$ are well reproduced. Moreover, the intensity ratio of [C II] to CO within the 4 kpc ring is the same as that of the latitudinal profiles (Fig. 4a).

These facts suggest that the intensity distributions of [C II] and CO are intimately correlated with each other in the inner Galactic disk. The [C II] longitudinal profile resembles that of the far-infrared continuum, too, though the [C II] intensity relative to the FIR appears to be slightly larger in the longitudinal profile than in the latitudinal profile. On the other hand, the longitudinal profile of H I 21 cm is totally different from that of [C II].

3.6. Contribution of the Discrete [C II] Sources to the Total [C II] Emission

In this subsection we estimate the contribution of the discrete [C II] sources to the total [C II] luminosity in the inner Galactic disk.

The “31° region” around W43 (§ 3.2) is a good region to make this estimate because the scan paths in this region are relatively close to each other, resulting in reliable contours (Fig. 3). The most intense object in this region is the W43 H II region itself. At a distance of 6 kpc from the Sun (Downes et al. 1980), the total FIR luminosity of the central $10'$ region is $2.4 \times 10^6 L_\odot$ (Lester et al. 1985).

By inspection of Figure 1a, we assign a [C II] intensity of $2.5 \times 10^{-4} \text{ ergs cm}^{-2} \text{ s}^{-1} \text{ sr}^{-1}$ to the $10'$ diameter region associated with W43. The [C II] luminosity of W43 is, then, $1800(\pm 500) L_\odot$, and the [C II]/FIR ratio $0.075(\pm 0.015)\%$ is in agreement with this ratio for other active star-forming regions (Stacey et al. 1990). Integrating over the entire 31° region, the observed total [C II] luminosity amounts to $3.1(\pm 0.9) \times 10^5 L_\odot$ (assuming a distance of 6 kpc), so that the contribution from W43 itself is only 0.6% of the total [C II] luminosity.

In this region ($30^\circ < l < 32^\circ$ and $|b| < 1^\circ$), there are 16 discrete H II regions other than W43 in the 5 GHz radio catalog (Altenhoff et al. 1978; Haynes et al. 1979), each having more than 100 Jy in the 100 μm band of *IRAS* point sources. The sum of the far-infrared intensities of these H II regions is just comparable to that of W43 (40,000 Jy in the *IRAS* 100 μm band). Recent observational and theoretical studies (Crawford et al. 1985; Tielens & Hollenbach 1985; Genzel et al. 1989; Wolfire, Hollenbach, & Tielens, 1989; Stacey et al. 1990) show that the ratio of [C II] luminosity to far-infrared luminosity in photodissociation regions ranges from 0.01% to 1% for Galactic and extragalactic objects. Therefore, even if the [C II]/FIR ratios for these sources is among the highest of the observed ratios (1%), their contribution is less than 8% of the total (diffuse and discrete) [C II] emission of this “31° region.”

We conclude that most [C II] emission of the Galactic disk is radiated not from discrete sources but from more extended and diffuse regions.

3.7. Total [C II] Luminosity of the Galaxy

To obtain the integrated [C II] luminosity of the Galaxy, we first derive a surface emissivity distribution, $\sigma(R)$, observed from the direction perpendicular to the Galactic disk as a function of the galactocentric distance, R (assuming axial symmetry around the Galactic rotation axis). Then we can relate the surface emissivity to the observed longitudinal distribution of Figure 5a [denoted by $f(l)$], as follows:

$$f(l) = \int_0^{\infty} \frac{\sigma(R)}{4\pi x} dx,$$

where x is the distance from the Sun on the line of sight at l . We can determine $\sigma(R)$ from $f(l)$ by the above equation. For simplicity, we divided the Galactic disk into concentric annuli of 0.5 kpc width from $R = 0$ to $R = 7.5$ kpc and assumed that the [C II] emissivity is constant in each annulus. We then calculated the above expression at directions in which the line of sight is tangent to the ring having the average radius of each annulus (0.25, 0.75, 1.25, 1.75, ..., 7.25 kpc). The surface emissivity of Figure 6 is a solution for $\sigma(R)$ which reproduces the fitted longitudinal distribution, $f(l)$, of Fig. 5a. The dashed line in $R < 4$ kpc indicates the interpolated part of the [C II] longitudinal profile between $l = 10^\circ$ and $l = 30^\circ$, where there are no observational data.

Integrating the surface emissivity, $\sigma(R)$, from $R = 0.5$ to $R = 7.5$ kpc, we obtain $2.7 \times 10^7 L_\odot$, or the total luminosity within $\pm 40\%$ error, which is dominated by the absolute calibration uncertainty ($\pm 30\%$) and by the zero-level uncertainty ($\pm 10\%$). If the surface emissivity between 7.5 and 8.5 kpc is constant and the same as that at 7.5 kpc, the [C II] luminosity of this annular region is $1.2 \times 10^6 L_\odot$. Therefore the value of $2.8 (\pm 1.1) \times 10^7 L_\odot$ is obtained for the [C II] luminosity from $R = 0.5$ to $R = 8.5$ kpc. This value is slightly lower than derived by Stacey et al. (1985), $4 \times 10^7 L_\odot$. However, because of their insufficient sky coverages, they assumed uniform [C II] emissivity inside the solar circle, which is clearly inconsistent with the observed results shown in Figure 5a. We have not included the contribution of the Galactic center to the total [C II] luminosity, since its contribution is small (Okuda et al. 1989; Mizutani et al. 1991).

The total far-infrared luminosity of the Galactic disk within the solar circle is estimated to be $7.6 \times 10^9 L_\odot$ within $R = 1.7$ to $R = 8.5$ kpc (Cox & Mezger 1988). The ratio of [C II] luminosity to far-infrared luminosity is, therefore, $0.36^{+0.28}_{-0.17}\%$.

This value for the luminosity ratio [C II]/FIR, $0.36^{+0.28}_{-0.17}\%$,

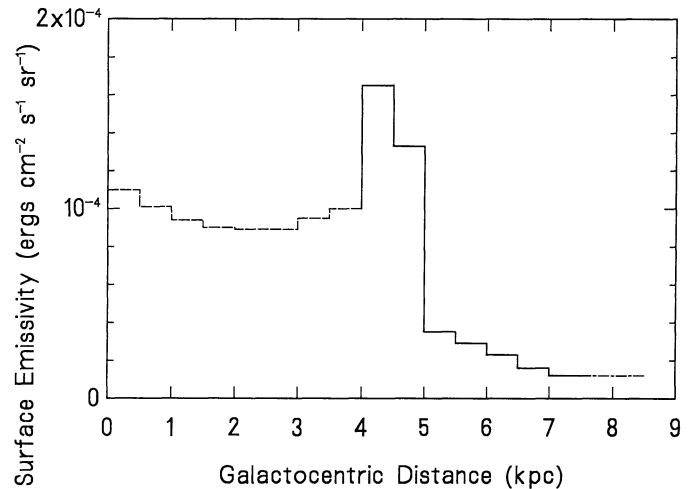


FIG. 6.—Surface emissivity of [C II] 158 μm from the Galactic disk as a function of galactocentric distance. This profile is derived from the smoothed longitudinal profile of Fig. 5a, assuming an axial symmetry in the [C II] emission distribution. The dashed line corresponds to the interpolated part of the longitudinal profile in Fig. 5a, and the dash-dot line indicates the assumed constant surface emissivity between $R = 7.5$ and $R = 8.5$ kpc.

agrees well with the intensity ratio $0.58^{+0.34}_{-0.24}\%$ derived in § 3.3 from the best-fit latitudinal profiles. The reason why the former ratio is slightly smaller than the latter ratio is probably that we neglect the discrete FIR peaks in the profile fitting. The derived total luminosity ratio of [C II]/FIR, $0.36^{+0.28}_{-0.17}\%$, is about average for external galaxies (Crawford et al 1985; Stacey et al. 1990).

4. DISCUSSION A: ORIGIN OF THE [C II] LINE RADIATION

In this section we calculate the expected [C II] intensities of the major components of the Galactic interstellar gas. The results will be qualitatively compared with the observed intensity ratios listed in Table 2. Parameters used are listed in Table 3.

It is assumed that the [C II] 158 μm line is optically thin, because the [C II] optical depth is less than unity for typical conditions in the [C II] emitting region of density $< 1000 \text{ cm}^{-3}$, temperature $< 300 \text{ K}$, $A_V < 2 \text{ mag}$, and $\Delta V > 4 \text{ km s}^{-1}$, and because the previous observational work (Stacey et al. 1985; Crawford et al. 1985) has indicated that the [C II] line from the extended region is optically thin.

TABLE 3

ADOPTED PARAMETERS FOR CALCULATION

Parameter	Adopted Value	Reference
[C]/[H]	3.6×10^{-4}	1
[C ⁺]/[C]	{ 0.5 (H I, H II regions and PDRs) < 0.1 (CO molecular clouds)	2
$N(\text{H})/E_{B-V}$	$5.8 \times 10^{21} \text{ cm}^{-2}/\text{mag}$	3
A_V/E_{B-V}	3.1	
$N(\text{H})/\int T(\text{H}1)dv$	$1.82 \times 10^{18} \text{ cm}^{-2}/(\text{K km s}^{-1})$	4
$N(\text{H}_2)/\int T(\text{CO})dv$	$3.6 \times 10^{20} \text{ cm}^{-2}/(\text{K km s}^{-1})$	5
Strength of UV radiation field in the solar neighborhood	$1.6 \times 10^{-3} \text{ ergs cm}^{-2} \text{ s}^{-1}$	6
$A_{(6-13.6 \text{ eV})}/A_V$	1.8	7

REFERENCES.—(1) Anders & Grevesse 1989; (2) van Dishoeck & Black 1988; (3) Bohlin, Savage, & Drake 1978; (4) Burton & de Lintell-Hekkert 1985; (5) Sanders, Solomon, & Scoville 1984; (6) Habing 1968; (7) de Jong et al. 1980.

4.1. Neutral Hydrogen Gas

The H I gas is not likely to be a major contributor to the [C II] emission, since the distribution of the atomic gas is so dissimilar to the [C II] distribution. However, it is valuable to estimate the contribution of the H I gas to the [C II] at $b = 0^\circ$ (Table 2). The excitation calculation was done in the same manner as that in Melnick et al. (1986). Figure 7 illustrates the expected [C II] cooling rate as a function of the hydrogen density, $n(\text{H})$, and the kinetic temperature, T_k . The dashed line represents the cooling rate required by our observations.

For the representative condition of the H I gas, $n(\text{H}) = 40 \text{ cm}^{-3}$ and $T_k = 70 \text{ K}$ (Salpeter 1979), the cooling rate per hydrogen atom by the [C II] line is about $3 \times 10^{-26} \text{ ergs s}^{-1}$. This is only 7% of $4.6_{-1.6}^{+2.1} \times 10^{-25} \text{ ergs s}^{-1}$ derived from the observed intensity ratio (Table 2). Therefore, the contribution of the H I gas to the observed [C II] intensity is negligible (see also Stacey et al. 1985; Crawford et al. 1985).

Pottasch, Wesselius, & van Duinen (1979) derived the [C II] cooling rate for diffuse H I clouds of $(0.7-1.6) \times 10^{-25} \text{ ergs s}^{-1}$ from UV absorption measurements. Their value is higher than the cooling rate calculated above, but lower than the measured cooling rate by a factor of 2.

4.2. Molecular Clouds

Next, we estimate the contribution of the molecular gas traced by $^{12}\text{CO}(J=1-0)$ to the extended [C II] emission. The excitation calculation was done again in the same manner as that of Melnick et al. (1986), and the [C II] cooling rates are illustrated in Figure 8, where it is assumed that the [C II] line is optically thin again and that $[\text{C}^+]/[\text{C}] = 0.1$. Since the average $[\text{C}^+]/[\text{C}]$ ratio is expected to be significantly less than 0.1 in the molecular cloud (de Jong et al. 1980; Tielens & Hollenbach 1985; van Dishoeck & Black 1988), the calculated cooling rate should be considered as an upper limit.

For typical conditions of giant molecular clouds (GMCs), $n(\text{H}_2) = 1000 \text{ cm}^{-3}$ and $T_k = 10 \text{ K}$ (Salpeter 1979), the [C II] cooling rate per hydrogen nucleus is considerably smaller than the observed value (*dashed line*) of $4.2_{-1.6}^{+1.9} \times 10^{-26} \text{ ergs s}^{-1}$ derived from the intensity ratio in Table 2. Therefore, the

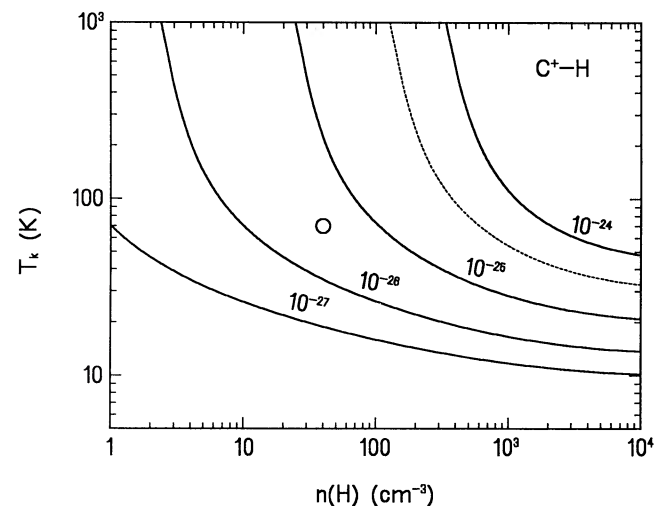


FIG. 7.—Cooling rate per hydrogen atom by the [C II] 158 μm emission line excited by collisions with hydrogen atoms (*solid lines*). The units are $\text{ergs s}^{-1} (\text{H atom})^{-1}$. The dashed line indicates the required cooling rate derived from the present observations, and the open circle indicates the typical conditions of H I clouds (Salpeter 1978).

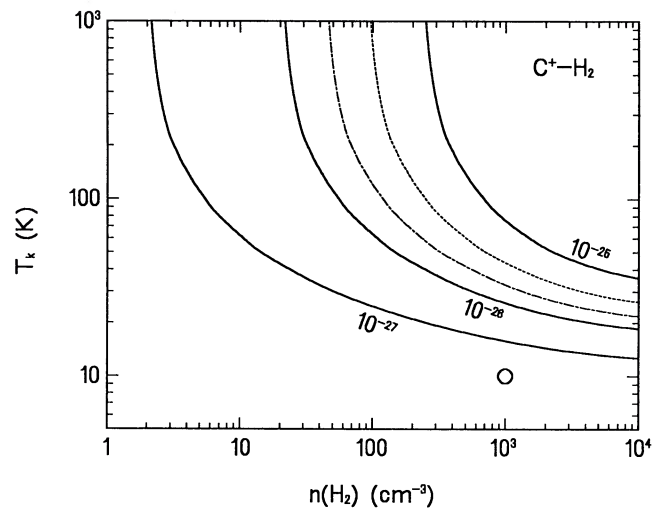


FIG. 8.—Cooling rate per hydrogen nucleus by the [C II] 158 μm line excited by collisions with hydrogen molecules (*solid lines*). The units are $\text{ergs s}^{-1} (\text{H nucleus})^{-1}$. The dashed line indicates the required cooling rate for the CO molecular gas derived from the present observations ($[\text{C}^+]/[\text{C}] = 0.1$), and the open circle indicates typical conditions of CO molecular clouds (Salpeter 1979). The dash-dot line indicates the required cooling rate for the C^+ region in the PDR surrounding the molecular cloud, assuming that $[\text{C}^+]/[\text{C}] = 0.5$ and the mass of the C^+ region is 40% of the CO molecular gas (see text), and the dash-dot line indicates $1.05 \times 10^{-25} \text{ ergs s}^{-1} (\text{H nucleus})^{-1}$.

molecular clouds traced by $^{12}\text{CO}(J=1-0)$ also cannot account for the observed [C II] intensity (see also Stacey et al. 1985; Crawford et al. 1985).

4.3. Extended Low-Density H II Region

Extended low-density (ELD) ionized gas is the third candidate for the [C II] emitting gas. According to Mezger (1978), typical conditions of the ELD H II regions are electron density $n_e \sim 3 \text{ cm}^{-3}$ and electron temperature $T_e \sim 7000 \text{ K}$. The method of the excitation calculation is essentially the same as that of the previous work (Stacey et al. 1985; Melnick et al. 1986) except that newer data are used for the collision strength (Hayes & Nussbaumer 1984). For $T_e = 7000 \text{ K}$ and n_e very much less than the critical density for this transition (about 30 cm^{-3}), the [C II] intensity is given by

$$\begin{aligned} I_{[\text{C II}]} &= \frac{1}{4\pi} L(T_e) n(\text{C}^+) n_e l \\ &= \frac{1}{4\pi} L(T_e) n_e^2 l \frac{[\text{C}^+]}{[\text{H}]} \\ &= 2.2 \times 10^{-26} n_e^2 l \text{ ergs cm}^{-2} \text{ s}^{-1} \text{ sr}^{-1}, \end{aligned}$$

where $L(T)$ is the cooling function for the temperature T and l is the length of ionized gas in the line of sight. The brightness temperature of the 5 GHz radio continuum of the free-free emission is written as follows (Spitzer 1978, § 3.5):

$$\begin{aligned} T_b &= \frac{\lambda^2}{2k_B} j_\nu l \\ &= 4.15 \times 10^{-23} n_e^2 l \text{ K}, \end{aligned}$$

where k_B is Boltzmann's constant, λ is the wavelength, and j_ν is the source function of the free-free emission. Therefore, the ratio of these two is independent of the emission measure, $n_e^2 l$, if $n_e \ll n_{\text{crit}}$, and otherwise depends weakly on T_e and n_e . Figure

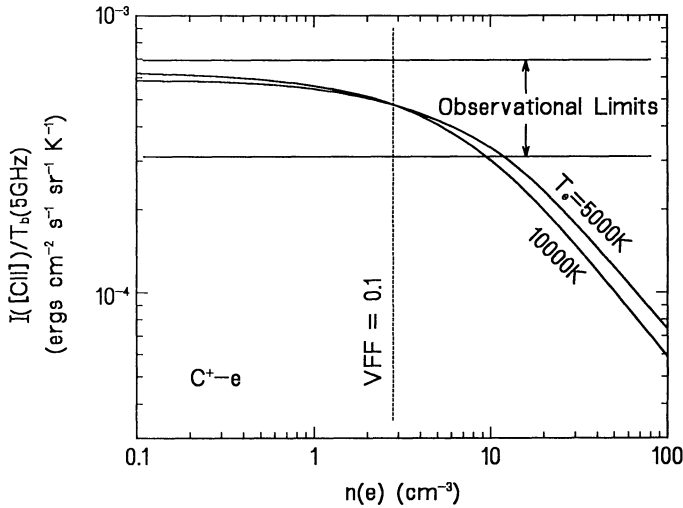


FIG. 9.—Ratio of the [C II] 158 μm intensity to the 5 GHz radio continuum brightness temperature. The [C II] line is assumed to be excited by collisions with electrons. The bounds in the observed ratio are indicated by the two horizontal lines. The vertical dashed line indicates the density assuming that the volume filling factor (VFF) of the ELD H II region is 10% inside the solar circle and 0% outside the solar circle.

9 represents the expected ratio $I_{[\text{C II}]} / T_b$ as a function of n_e . For low densities, the calculated ratio is $I_{[\text{C II}]} / T_b \sim 6 \times 10^{-4}$ (ergs $\text{cm}^{-2} \text{s}^{-1} \text{sr}^{-1} / \text{K}$). The observed intensity ratio of $I_{[\text{C II}]} / T_b$ (Table 2) is $4.8^{+2.1}_{-1.7} \times 10^{-4}$ (ergs $\text{cm}^{-2} \text{s}^{-1} \text{sr}^{-1} / \text{K}$), consistent with the calculated value as long as $n_e < 10 \text{ cm}^{-3}$. We therefore suggest that the ELD ionized gas may account for a substantial fraction of the observed [C II] line emission. However, as pointed out by Stacey et al (1985), if C^+ is depleted in the ELD, the ELD ionized gas cannot account for the observed [C II] emission.

4.4. Photodissociation Regions

Finally, we calculated the expected intensity of the [C II] emission from the photodissociation regions (PDRs) formed on the surface of interstellar clouds which are illuminated externally by the interstellar UV radiation field. Near the surface of the cloud, CO molecules are photodissociated into carbon and hydrogen atoms, and then the carbon atoms are immediately ionized. Consequently, nearly all gaseous carbon is in the form of C^+ ions (C^+ region). The thickness of the C^+ region (from the surface to the $\text{C}^+/\text{C}^0/\text{CO}$ transition region) depends on the gas density and the incident UV radiation field. De Jong et al. (1980) and van Dishoeck & Black (1988) showed this thickness to be about 1 and 0.6 mag in A_V , respectively, for densities from 100 to 1000 cm^{-3} and for UV radiation fields similar to the solar neighborhood. The difference between the two estimates is probably caused by the assumed gas density.

We adopt the plane-parallel geometry as in previous work (de Jong et al. 1980; Tielens & Hollenbach 1985), and assume that the density ranges between 100 and 1000 cm^{-3} .

Previous work (de Jong et al. 1980; Tielens & Hollenbach 1985; Burton, Hollenbach, & Tielens 1989) has shown that for moderate densities ($n \leq 10^4 \text{ cm}^{-3}$) the dominant gas-heating process in C^+ regions is photoelectric ejection of energetic electrons from grains. Only photons of $6 \text{ eV} < h\nu < 13.6 \text{ eV}$ are effective for the photoelectric gas heating because the photons above 13.6 eV are absorbed in H II regions and photons below 6 eV cannot transfer enough energy to the

electron to overcome the photoelectric threshold of the dust grain (6 eV; de Jong 1980).

The strength of the incident UV radiation field is denoted by G_{UV} measured in units of the equivalent Habing (1968) flux of the solar neighborhood ($1.6 \times 10^{-3} \text{ ergs cm}^{-2} \text{ s}^{-1}$, $6 \text{ eV} \leq h\nu \leq 13.6 \text{ eV}$, as shown in Table 3). In the inner Galactic disk, G_{UV} is expected to be much larger than unity because of the higher stellar density as compared with that of the solar neighborhood. On the other hand, integrated through the Galactic plane, G_{UV} is not likely to be as large as near luminous star(s) ($\sim 10^4$ – 10^5). We assume that the incident UV field ranges from $G_{\text{UV}} = 1$ to $G_{\text{UV}} = 100$.

For moderate temperatures and densities ($n < 10^3 \text{ cm}^{-3}$ and $T < 300 \text{ K}$), the dominant gas cooling process is the [C II] 158 μm line for C^+ regions illuminated by UV fields of $G_{\text{UV}} = 1$ to $G_{\text{UV}} = 100$ (de Jong et al. 1980; Tielens & Hollenbach 1985; van Dishoeck & Black 1988). In the steady state, the [C II] intensity as the dominant cooling process should nearly equal the integral of the photoelectric heating rate along the line of sight in the C^+ region. Therefore,

$$I_{[\text{C II}]} \simeq \frac{1}{4\pi} \int_0^{s(\text{C}^+)} \Gamma_d ds,$$

where Γ_d is the photoelectric heating rate (de Jong et al. 1980; Tielens & Hollenbach 1985), s is the distance from the surface, and $s(\text{C}^+)$ is the distance to the $\text{C}^+/\text{C}^0/\text{CO}$ transition region. The above formula can easily be evaluated by

$$I_{[\text{C II}]} \simeq 5(\pm 1) \times 10^{-5} G_{\text{UV}} E_{\text{PH}} \{1 - \exp[-1.8A_V(\text{C}^+)]\} \text{ ergs cm}^{-2} \text{ s}^{-1} \text{ sr}^{-1},$$

where E_{PH} is the photoelectric heating efficiency, and $A_V(\text{C}^+)$ is the optical depth from the surface to the $\text{C}^+/\text{C}^0/\text{CO}$ transition region. The upper bound of numerical factor in the above expression comes from the photoelectric heating rate given by de Jong et al. (1980), and the lower from Tielens & Hollenbach (1985). In the following analysis, E_{PH} is assumed to be 0.03, which is a reasonable value for $G_{\text{UV}} < 100$ according to Tielens & Hollenbach (1985). This equation expresses the [C II] intensity observed from the perpendicular direction to the photodissociating layer.

Next, consider spherical molecular clouds enveloped with C^+ region mantles (the number of the cloud is defined by N_c) in order to evaluate the mean [C II] intensity in one cloud. If we observe a spherical C^+ mantle surrounding the spherical molecular cloud of diameter r at a distance D , the total [C II] intensity is approximately $(4\pi r^2/D^2)I_{[\text{C II}]}$, neglecting the thickness of the mantles. Dividing it by the solid angle, $\pi r^2/D^2$, the mean intensity per cloud, $I_{[\text{C II}]}^{\text{mean}}$, is $4I_{[\text{C II}]}$ (see also Wolfire, Tielens, & Hollenbach 1990):

$$I_{[\text{C II}]}^{\text{mean}} \simeq 2(\pm 0.4) \times 10^{-4} N_c G_{\text{UV}} E_{\text{PH}} \{1 - \exp[-1.8A_V(\text{C}^+)]\} \simeq 6(\pm 1.2) \times 10^{-6} N_c G_{\text{UV}} \text{ ergs cm}^{-2} \text{ s}^{-1} \text{ sr}^{-1},$$

where the exponential term is set to zero because $A_V(\text{C}^+)$ is expected to be more than 1 mag. The mean free path of molecular clouds in the inner Galaxy is about 3 kpc (Sanders, Scoville, & Solomon 1985). We therefore expect about five molecular clouds ($N_c \simeq 5$) along the line of sight in the direction of W43. The observed [C II] intensity at $b = 0^\circ$ except for the contribution of W43 itself is about $7(\pm 2) \times 10^{-4} \text{ ergs cm}^{-2} \text{ s}^{-1} \text{ sr}^{-1}$ (Fig. 1a). Therefore, we obtain $G_{\text{UV}} \sim 23^{+15}_{-9}$. Note that the derived G_{UV} is inversely proportional to the

photoelectric heating efficiency which was theoretically estimated. The above discussion does not involve large uncertainties that might arise in the theoretical estimation of the efficiency.

Consequently, the [C II] intensity at $b = 0^\circ$ can be explained by the model that has five spherical molecular clouds along the line of sight illuminated by interstellar UV radiation of 23 times the local interstellar radiation field.

5. DISCUSSION B: NATURE OF DIFFUSE PHOTODISSOCIATION REGION

5.1. Extended [C II] Emission from Diffuse Photodissociation Region

The most natural origin for the observed [C II] radiation is the photodissociation regions formed on the surfaces of UV exposed giant molecular clouds in the inner Galactic disk. Cox & Mezger (1989), from an analysis of the *IRAS* data, conclude that most of the diffuse far-infrared luminosity (about 70%) arises from the dust associated with the diffuse atomic hydrogen or located in the outer layer of molecular clouds which are heated by the general interstellar radiation field. The fact that the [C II] emission is correlated with the 100 μm continuum emission supports this model.

Several authors have found the diffuse [C II] emission regions extended over a wide region around the H II regions of M42, M17, and NGC 2024 (Russell et al. 1981; Kurtz et al. 1983; Stutzki et al. 1988; Matsuhara et al. 1989, 1990). These extended emission regions are clearly distinguished from more compact and intense [C II] emission regions because of their larger spatial extents, lower intensities, and uniform spatial distribution. The intensities of these extended emission components (a few times 10^{-4} ergs cm^{-2} s^{-1} sr^{-1}) are similar to that of the large-scale [C II] emission in the inner Galactic disk. The large-scale [C II] emission may, therefore, be interpreted as superposition of one or more of these extended emission regions. The conclusions presented here are therefore consistent with those of Crawford et al. (1985) and Stacey et al. (1985). Much of the observed [C II] line emission arises from the photodissociated envelopes of giant molecular clouds.

5.2. Estimation of C^+ Gas Mass

We estimate the mass fraction contained in the C^+ region relative to that contained in the CO molecular gas. The total column mass of the CO gas in the line of sight toward W43 is estimated from the integrated CO intensity by using the conversion factor listed in Table 3. Since the integrated CO intensity is about 300 K km s^{-1} (Fig. 4a), the column mass expressed in A_V is 114 mag. Dividing it by the number of clouds, $N_C = 5$ (see § 4.4), the average A_V per cloud is 23 mag. If the density in the spherical cloud is constant, by a straightforward calculation, $A_V(\text{CO})$ between the center and the edge (the radius expressed in A_V) is derived to be $\frac{3}{4}A_V$ on average, i.e., 17 mag.

Next we estimate the thickness of the C^+ region. $A_V(\text{C}^+)$ for the density of 1000 cm^{-3} and $G_{\text{UV}} = 1$ is 0.6 mag (van Dishoeck & Black 1988). Assuming that the inner boundary of the C^+ layer is determined by the strength of the UV field there, then $A_V(\text{C}^+)$ for higher G_{UV} can be obtained approximately by extrapolation according to

$$A_V(\text{C}^+) \simeq 0.6 + [2.5 \log_{10}(G_{\text{UV}})]/1.8 \text{ mag}$$

where the value 1.8 is the ratio of the absorption rate for UV

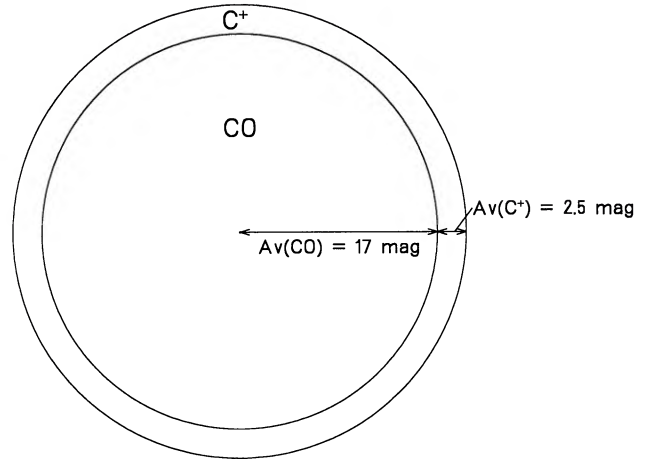


FIG. 10.—Schematic picture of a model molecular cloud illuminated by the interstellar UV radiation of $G_{\text{UV}} \sim 23$, by which the C^+ region is formed in the outer part.

photons relative to that for visual photons (see Table 3); then we obtain $A_V(\text{C}^+) = 2.5(\pm 0.3)$ mag for $G_{\text{UV}} = 23^{+1.5}_{-9}$. For our model cloud, then, the radius of the CO gas region is 17 mag and the thickness of the C^+ region is $2.5(\pm 0.3)$ mag (Fig. 10).

Now we can evaluate the mass ratio of the C^+ gas to the CO gas [$M(\text{C}^+)/M(\text{CO})$] under the assumption that the thickness of the C^+ layer is negligible compared with that of the CO region, as follows:

$$\begin{aligned} \frac{M(\text{C}^+)}{M(\text{CO})} &\simeq \frac{4\pi A_V(\text{CO})^2 A_V(\text{C}^+)}{(4\pi/3)A_V(\text{CO})^3} \\ &= \frac{3A_V(\text{C}^+)}{A_V(\text{CO})}. \end{aligned}$$

For $A_V(\text{CO}) = 17$ mag and $A_V(\text{C}^+) = 2.5(\pm 0.3)$ mag, the mass ratio is $\sim 44(\pm 5)\%$.

For larger $N_C (> 5)$ and, consequently, smaller G_{UV} , the mass ratio of the C^+ gas to the CO gas *increases*, because $A_V(\text{C}^+)$ does not decrease as rapidly as G_{UV} . Even if only a half of the diffuse [C II] intensity is attributed to the C^+ region, then $G_{\text{UV}} \simeq 11.5$, $A_V = 2.1$ mag, the mass ratio is equal to 37%.

We conclude that there are C^+ regions around each molecular cloud, illuminated by a radiation field $23^{+1.5}_{-9}$ times more intense than those in the solar neighborhood, and the total mass of this region amounts to up to 35%–50% of the molecular gas mass as traced by its $^{12}\text{CO}(J = 1-0)$ emission.

5.3. Estimation of Typical Temperature and Density

If the [C II] comes from C^+ regions which contain $\sim 40\%$ of the CO gas, then the cooling rate per hydrogen nucleus in these C^+ regions is 1.05×10^{-25} ergs s^{-1} . From Figure 8, effective physical properties of the C^+ regions to give this cooling rate are $n(\text{H}_2) \simeq 100 \text{ cm}^{-3}$ and $T \simeq 100$ K. This set of parameters is reasonable for surface regions of molecular clouds, since the density is smaller than in molecular clouds yet larger than the density of diffuse hydrogen clouds, and the temperature is higher than in molecular clouds yet lower than in ELD ionized gas.

Wolfire et al. (1989) outline a method based on photodissociation region models for estimating cloud densities and UV field strengths from the observed intensity ratios $I_{[\text{C II}]/I_{\text{IR}}}$ and $I_{\text{CO}}/I_{\text{IR}}$. The observed intensity ratios are $0.0058^{+0.0034}_{-0.0024}$

and $3.8^{+1.4}_{-0.9} \times 10^{-6}$, respectively, for which we obtain $n \leq 10^5 \text{ cm}^{-3}$ and $G_{\text{UV}} \simeq 30$. These values are consistent with our results described above.

Stacey et al. (1985) required a higher density, 300 cm^{-3} , and a higher temperature, 300 K, for the surface of the molecular clouds at $l = 2^\circ$ and $l = 7^\circ$ in order to explain the brightness of their [C II] observations. The smaller densities and temperatures arrived at here are the result of differences in the assumed C^+ abundance, the geometry of the PDR layer, and the observed area of the sky.

5.4. Correlations of [C II] with FIR and 5 GHz Emission

Since photodissociation regions convert most of the incident UV and/or visual radiation energy into far-infrared, both continuum and lines, the correlation between the [C II] and FIR emission is naturally understood.

The correlation between the [C II] and the radio continuum can be understood if the ELD H II regions (§ 4.3) are a primary source of the diffuse [C II] emission. However, if the ELD ionized gas is the primary source of the [C II] emission, then the observed excellent correlation between the [C II] and CO emission is left unexplained.

An interesting interpretation of the observed [C II]/radio continuum correlation is that extended PDRs are associated with ELD H II regions. For example, in the case of a molecular cloud exposed to an external UV radiation field, both (ELD) H II regions and photodissociation regions may form on the surface of the molecular cloud. This picture of the interstellar medium explains all of the observed correlations presented here. In this case, a certain portion of the observed [C II] intensity may arise in the ELD H II region and the rest in the photodissociation region.

6. CONCLUSIONS

We have obtained the first observational result of the Galactic [C II] emission over broad regions of the sky. We find the following:

1. In the inner Galactic disk, there exists large-scale [C II] emission which is not associated with discrete H II regions. This extended [C II] emission is not resolved into smaller structure with the 3/4 beam.

2. This extended [C II] emission dominates the total [C II] luminosity of the inner Galactic disk.

3. The [C II] intensity tracks that of $^{12}\text{CO}(J = 1-0)$.

4. A significant portion of the diffuse [C II] emission of the Galactic plane is radiated from C^+ regions in the photodissociation layers surrounding the molecular clouds illuminated by the general interstellar UV radiation field. The average strength of the UV field is $\sim 23^{+15}_{-9}$. The extended low-density ionized gas may be another source of the diffuse [C II] emission.

5. The mass of the [C II] emitting gas probably amounts to as much as 35%–50% of the molecular gas traced by $^{12}\text{CO}(J = 1-0)$.

6. The total [C II] luminosity of the Galaxy is about $2.8(\pm 1.1) \times 10^7 L_\odot$, or $0.36^{+0.28}_{-0.17}$ % of the total far-infrared luminosity.

We thank the staff of NSBF at Palestine for their expertise in this project (flight numbers 1464p and 1465p) and Professor W. B. Burton and D. B. Sanders for providing H I data and CO data on a magnetic tape. We are grateful to M. Narita, H. Takami, and the balloon group of ISAS for developing the instruments with us, and are greatly appreciative of Gordon J. Stacey's valuable suggestions. F. J. L. and T. N. wish to thank N. W. Boggess and F. C. Gillett for their support. This work has been supported by grants-in-aid from the Ministry of Education, Science, and Culture in Japan, by the Japan Society for the Promotion of Science, and in the United States by the National Science Foundation (INT-8613481) and by the National Aeronautics and Space Administration (NGR-03-002-269).

REFERENCES

- Altenhoff, W. J., Downes, D., Pauls, T., & Schraml, J. 1978, *A&AS*, 35, 23
 Anders, E., & Grevesse, N. 1989, *Geochim. Cosmochim. Acta*, 53, 197
 Bohlin, R. C., Savage, B. D., & Drake, J. F. 1978, *ApJ*, 224, 132
 Burton, M., Hollenbach, D., & Tielens, A. G. G. M. 1989, in *ESLAB Symposium 22, Infrared Spectroscopy in Astronomy*, ed. B. H. Kadeich (ESA SP-290), 141
 Burton, W. B. 1985, *A&AS*, 62, 365
 Burton, W. B., & te Lintel-Hekkert, P. 1985, *A&AS*, 62, 645
 Cooksy, A. L., Blake, G. A., & Saykally, R. J. 1986, *ApJ*, 305, L89
 Cox, P., & Mezger, P. G. 1988, in *Third Internat. IRAS Conf., Comets to Cosmology*, ed. E. Lawrence (Berlin: Springer-Verlag), 97
 ———. 1989, *Astr. Ap. Rev.*, 1, 49
 Crawford, M. K., Genzel, R., Townes, C. H., & Watson, D. M. 1985, *ApJ*, 291, 755
 Dame, T. M. et al. 1987, *ApJ*, 322, 706
 de Jong, T. 1980, *Highlights Astr.*, 5, 301
 de Jong, T., Dalgarno, A., & Boland, W. 1980, *A&A*, 91, 68
 Downes, D., Wilson, T. L., Bieging, J., & Wink, J. 1980, *A&AS*, 40, 379
 Genzel, R., Harris, A. I., & Stutzki, J. 1989, in *ESLAB Symposium 22, Infrared Spectroscopy in Astronomy*, ed. B. H. Kadeich (ESA SP-290), 115
 Habing, H. J. 1968, *Bull. Astr. Inst. Netherlands*, 19, 421
 Hayes, M. A., & Nussbaumer, H. 1984, *A&A*, 134, 193
 Haynes, R. F., Caswell, J. L., & Simons, L. W. J. 1978, *Australian J. Phys. Ap. Suppl.*, 45, 1
 ———. 1979, *Australian J. Phys. Ap. Suppl.*, 48, 1
 Hiromoto, N., Itabe, T., Aruga, T., Okuda, H., Matsuhara, H., Shibai, H., Nakagawa, T., & Saito, M. 1989, *Infrared Phys.*, 29, 255
IRAS Cataloged Galaxies and Quasars. 1985, ed. C. J. Lonsdale, G. Helou, J. C. Good, & W. Rice (JPL D-1932)
IRAS Catalogs and Atlases: Explanatory Supplement. 1985, ed. C. A. Beichman, G. Neugebauer, H. J. Habing, P. E. Clegg, & T. J. Chester (Washington, DC: GPO)
- Kurtz, N. T., Smyers, S. D., Russell, R. W., Harwit, M., & Melnick, G. 1983, *ApJ*, 264, 538
 Lester, D. F., Dinerstein, H. L., Werner, M. W., Harvey, P. M., Evans II, N. J., & Brown, R. L. 1985, *ApJ*, 296, 565
 Matsuhara, H., et al. 1989, *ApJ*, 339, L67
 Matsuhara, H., et al. 1990, *Proc. Pacificchem '90*, No. 228, *Chemistry and Spectroscopy of Interstellar Molecules*, ed. S. Saito, N. Kaifu, D. K. Bohme, & E. Herbst (Tokyo: Univ. Tokyo Press), in press
 McBreen, B., Jaffe, D. T., & Fazio, G. G. 1983, *AJ*, 88, 835
 Melnick, G., Stacey, G. J., Viscuso, P. J., & Fuller, C. E. 1986, *ApJ*, 303, 638
 Mezger, P. G. 1978, *A&A*, 70, 565
 Mizutani, K., et al. 1991, in preparation
 Nakagawa, T., Okuda, H., Shibai, H., Kobayashi, Y., & Matsuhara, H. 1990, in *Proc. SPIE*, Vol. 1235, *Instrumentation in Astronomy VII*, ed. D. L. Crawford, p. 97
 Nakagawa, T., et al. 1991, in preparation
 Okuda, H., et al. 1984, in *Proc. 14th Internat. Symposium Sp. Tech. Sci.*, ed. M. Nagatomo (Tokyo: AGNE), 1217
 Okuda, H., Shibai, H., Nakagawa, T., Kobayashi, Y., Matsumoto, T., Low, F. J., & Nishimura, T. 1986, in *Proc. SPIE*, Vol. 627, *Instrumentation in Astronomy VI*, ed. D. L. Crawford, p. 20
 Okuda, H., et al. 1989, in *IAU Symposium 136*, *The Center of the Galaxy*, ed. M. Morris (Dordrecht: Reidel), 145
 Pottasch, S. R., Wesselius, P. R., & van Duinen, R. J. 1979, *A&A*, 74, L15
 Reifenstein, E. C., III, Wilson, T. L., Burke, B. F., Mezger, P. G., & Altenhoff, W. J. 1970, *A&A*, 4, 357
 Russell, R. W., Melnick, G., Smyers, S. D., Kurts, N. T., Gosnell, T. R., Harwit, M., & Werner, M. W. 1981, *ApJ*, 250, L35
 Salpeter, E. E. 1979, in *IAU Symposium 84*, *The Large-Scale Characteristics of the Galaxy*, ed. W. B. Burton (Dordrecht: Reidel), 245
 Sanders, D. B., Clemens, D. P., Scoville, N. Z., & Solomon, P. M. 1986, *ApJS*, 60, 1

- Sanders, D. B., Scoville, N. Z., & Solomon, P. M. 1985, ApJ, 289, 373
Sanders, D. B., Solomon, P. M., & Scoville, N. Z. 1984, ApJ, 276, 182
Shibai, H. et al. 1990, in Proc. SPIE, Vol. 1235, Instrumentation in Astronomy VII, ed. D. L. Crawford, p. 108
Spitzer, L., Jr. 1978, Physical Processes in the Interstellar Medium (New York: Wiley)
Stacey, G. J., Geis, N., Genzel, R., Lugten, J. B., Poglitsch, A., Sternberg, A., & Townes, C. H. 1990, ApJ, submitted
Stacey, G. J., Viscuso, P. J., Fuller, C. E., & Kurtz, N. T. 1985, ApJ, 289, 803
Stutzki, J., Stacey, G. J., Genzel, R., Harris, A. I., Jaffe, D. T., & Lugten, J. B. 1988, ApJ, 332, 379
Tielens, A. G. G. M., & Hollenbach, D. 1985, ApJ, 291, 722
van Dishoeck, E. F., & Black, J. H. 1988, ApJ, 334, 771
Wolfire, M. G., Hollenbach, D., & Tielens, A. G. G. M. 1989, ApJ, 344, 770
Wolfire, M. G., Tielens, A. G. G. M., & Hollenbach, D. 1990, ApJ, 358, 116